



CHORUS

This is the accepted manuscript made available via CHORUS. The article has been published as:

First-principles studies of phase stability and crystal structures in Li-Zn mixed-metal borohydrides

Yongli Wang, Yongsheng Zhang, and C. Wolverton

Phys. Rev. B **88**, 024119 — Published 29 July 2013

DOI: [10.1103/PhysRevB.88.024119](https://doi.org/10.1103/PhysRevB.88.024119)

First-principles studies of phase stability and crystal structures in Li-Zn mixed-metal borohydrides

Yongli Wang, Yongsheng Zhang and C. Wolverton
Department of Materials Science and Engineering,
Northwestern University, Evanston, Illinois 60208, USA

We address the problem of finding mixed metal borohydrides with favorable thermodynamics and illustrate the approach using the example of $\text{LiZn}_2(\text{BH}_4)_5$. Using density functional theory (DFT), along with the grand canonical linear programming method (GCLP), we examine the experimentally and computationally proposed crystal structures and the finite-temperature thermodynamics of dehydrogenation for the quaternary hydride $\text{LiZn}_2(\text{BH}_4)_5$. We find the following: (i) For $\text{LiZn}_2(\text{BH}_4)_5$, DFT calculations of the experimental crystal structures reveal that the structure from the neutron diffraction experiments of Ravnsbæk *et al.* is more stable [by 24 kJ/(mol f.u.)] than that based on a previous X-ray study. (ii) Our DFT calculations show that when using the neutron-diffraction structure of $\text{LiZn}_2(\text{BH}_4)_5$, the recently theoretically predicted $\text{LiZn}(\text{BH}_4)_3$ compound is unstable with respect to the decomposition into $\text{LiZn}_2(\text{BH}_4)_5 + \text{LiBH}_4$. (iii) GCLP calculations show that even though $\text{LiZn}_2(\text{BH}_4)_5$ is a combination of weakly ($\text{Zn}(\text{BH}_4)_2$) and strongly (LiBH_4) bound borohydrides, its decomposition is not intermediate between the two individual borohydrides. Rather, we find that the decomposition of $\text{LiZn}_2(\text{BH}_4)_5$ is divided into a weakly exothermic step [$\text{LiZn}_2(\text{BH}_4)_5 \rightarrow 2\text{Zn} + \frac{1}{5}\text{LiBH}_4 + \frac{2}{5}\text{Li}_2\text{B}_{12}\text{H}_{12} + \frac{36}{5}\text{H}_2$], and three strong endothermic steps [$12\text{LiBH}_4 \rightarrow 10\text{LiH} + \text{Li}_2\text{B}_{12}\text{H}_{12} + 13\text{H}_2$; $\text{Zn} + \text{LiH} \rightarrow \text{LiZn} + \frac{1}{2}\text{H}_2$; $2\text{Zn} + \text{Li}_2\text{B}_{12}\text{H}_{12} \rightarrow 2\text{LiZn} + 12\text{B} + 6\text{H}_2$]. DFT-calculated $\Delta H_{ZPE}^{T=0K}$ values for the first three $\text{LiZn}_2(\text{BH}_4)_5$ decomposition steps are -19, +37, +74 kJ/(mol H_2) respectively. The behavior of $\text{LiZn}_2(\text{BH}_4)_5$ shows that mixed metal borohydrides formed by mixing borohydrides of high and low thermodynamics stabilities do not necessarily have an intermediate decomposition tendency. Our results suggest the correct strategy to find intermediate decomposition in mixed metal borohydrides is to search for stable mixed-metal products such as ternary metal borides.

I. INTRODUCTION

Utilizing hydrogen as a fuel is one promising avenue for the transition towards a reliable and low-emission energy system. However, a major challenge is to develop a safe and compact hydrogen storage system that has high gravimetric and volumetric H_2 density as well as fast H_2 desorption and absorption rates at moderate temperatures and pressures. Unfortunately, to date, no known materials have met these requirements. Recently, metal borohydrides have received considerable attention owing to their high hydrogen-storage capacities¹. For example, LiBH_4 , a typical alkali metal borohydride, has a theoretical gravimetric density of $\sim 18\%$, above the system target for passenger vehicles². However, the practical application of LiBH_4 is hindered by its high thermodynamic enthalpy³ and unfavorable kinetic properties⁴⁻⁶. However, other metal borohydrides, such as $\text{Zn}(\text{BH}_4)_2$, suffer from different limitations. $\text{Zn}(\text{BH}_4)_2$ ⁷, a transition metal borohydride, is unstable at room temperature and readily decomposes, accompanied with releasing diborane gas. The thermodynamic stability of binary metal hydrides has been found to be inversely related to the metal electronegativity⁸. A similar relationship for borohydrides has been theoretically as well as experimentally investigated^{1,9,10}. Unfortunately, efforts to tackle the drawbacks of the single cation borohydrides have not been completely successful.

It has been suggested that double-cation borohydrides^{11,12}, especially those formed by mix-

ing metal borohydrides of high and low thermodynamic stabilities, such as $\text{LiBH}_4 + \text{Zn}(\text{BH}_4)_2$, may bring new opportunities. Inspired by the hypothesis that it may be possible to precisely adjust the thermal stabilities of borohydrides by a careful choice of double- or multi-cations, Li *et al.*¹⁰ experimentally examined the thermodynamic stabilities of $\text{MLi}_{m-n}(\text{BH}_4)_m$ ($\text{M}=\text{Zn}$, $n=2$; $\text{M}=\text{Al}$, $n=3$; $\text{M}=\text{Zr}$, $n=4$; $n \leq m$). Also, Černý *et al.* have experimentally studied $\text{Mg}_x\text{Mn}_{(1-x)}(\text{BH}_4)_2$ ($x=0-0.8$)¹². However, these studies do not provide a clear path to tuning the thermodynamic properties of mixed-metal borohydride based hydrogen storage materials. For instance, Černý and the co-workers¹² found the decomposition temperature of $\text{Mg}_x\text{Mn}_{(1-x)}(\text{BH}_4)_2$ ($x=0-0.8$) does not vary significantly with Mg content (433-453 K). In another approach, Hummelshoj *et al.*¹³ performed a large-scale computational screening based on density functional theory (DFT) of combinations of mixed metal borohydrides. These authors investigated the stability and dehydrogenation of mixed metal borohydrides using model structures with various coordinations of the metal/ BH_4 ions. One particular result of reference¹³ is the prediction of a stable mixed Li-Zn borohydride phase.

Ravnsbæk *et al.*¹⁴ have synthesized this mixed borohydride by ball milling LiBH_4 and ZnCl_2 with ratio of 2.5:1. The two reactants follow the reaction $5\text{LiBH}_4 + 2\text{ZnCl}_2 \rightarrow \text{LiZn}_2(\text{BH}_4)_5 + 4\text{LiCl}$. The synthesized $\text{LiZn}_2(\text{BH}_4)_5$ was probed by synchrotron radiation powder X-ray diffraction (PXRD) and a candidate

crystal structure was identified by PXD. Following this work, Černý *et al.*¹⁵ performed a combination of *in situ* synchrotron powder diffraction and energy minimization (DFT) study on $\text{LiZn}_2(\text{BH}_4)_5$. The authors¹⁵ also proposed a new compound $\text{LiZn}(\text{BH}_4)_3$, though $\text{LiZn}(\text{BH}_4)_3$ is not observed experimentally at ambient pressure and in the temperature range of 100–400 K. Subsequently, motivated by these theoretical and experimental predictions, Aidhy *et al.* performed a phase stability study¹⁶ of Li-Zn mixed-metal borohydride compounds, using a combination of DFT and a recently developed crystal structure prediction method – the prototype electrostatic ground state (PEGS) method¹⁷. This theoretical DFT+PEGS work successfully predicted a low-energy $\text{LiZn}(\text{BH}_4)_3$ phase, which has a lower DFT energy than the two-phase mixture of $\text{Zn}(\text{BH}_4)_2$ and $\text{LiZn}_2(\text{BH}_4)_5$ in the previously mentioned PXD structure. Aidhy *et al.*¹⁶ only reported static DFT energies at $T=0\text{K}$, without considering vibrational contributions. They¹⁶ found surprisingly, the $\text{LiZn}_2(\text{BH}_4)_5$ phase obtained in the X-ray work¹⁴ was ~ 2 kJ/(mol cation) above the tie line between $\text{LiZn}(\text{BH}_4)_3$ and $\text{Zn}(\text{BH}_4)_2$, indicating either that: (i) the observed $\text{LiZn}_2(\text{BH}_4)_5$ phase is not stable, or (ii) the previously proposed PXD crystal structure of $\text{LiZn}_2(\text{BH}_4)_5$ is incorrect and hence the DFT energy (based on this structure) is artificially too high, leading to an incorrect prediction of its instability. Recently, Ravnsbæk *et al.*¹⁸ utilized powder neutron diffraction (PND) to revisit the crystal structure of $\text{LiZn}_2(\text{BH}_4)_5$. These authors found the structures of $\text{LiZn}_2(\text{BH}_4)_5$ studied by X-ray and neutron methods bear similar metal-boron positions, but with large differences in the hydrogen positions. These two proposed experimental structures raise many unanswered questions regarding the phase stability and thermodynamic reactions in the Li-Zn-BH₄ system: Which structure of $\text{LiZn}_2(\text{BH}_4)_5$ in the two experimental studies^{14,18} is more stable? Which phases/stoichiometries are ground states of the mixed Li-Zn borohydrides? What is the thermodynamic reaction pathway in the decomposition of the Li-Zn-BH₄ system?

In this paper, we answer these questions through a use of DFT calculations to obtain total crystal binding energies and vibrational free energies. We find (i) the DFT-relaxed $\text{LiZn}_2(\text{BH}_4)_5$ PND structure¹⁸ has a lower energy, thus is more stable [by 24 kJ/(mol f.u.)] than the PXD structure¹⁴; (ii) the theoretically predicted $\text{LiZn}(\text{BH}_4)_3$ structure¹⁶ is unstable with respect to the decomposition into LiBH_4 and $\text{LiZn}_2(\text{BH}_4)_5$, with or without including the vibrational contribution; (iii) for the decomposition of $\text{LiZn}_2(\text{BH}_4)_5$, the weakly-bound $\text{Zn}(\text{BH}_4)_2$ portion in this complex borohydride decomposes at low temperature, leaving the strongly-bound LiBH_4 .

II. METHODOLOGY

A. First-Principles Calculations

First-principles density functional theory^{19,20} calculations were performed using Vienna ab initio simulation package (VASP)²¹ code with a plane-wave method based on the Perdew-Wang (PW91) generalized gradient approximation²² and the core-valence electron interaction treated by Blöchl’s projector augmented wave (PAW) method^{23,24}. $1s^22s^1$, $3d^{10}4p^2$, and $2s^22p^1$ are treated as valence electrons in Li, Zn and B atoms, respectively. A high plane wave energy cutoff of 875 eV was used for the electronic wave functions. The k-point sampling was performed on a dense Monkhorst-Pack²⁵ grid with meshes of $4 \times 4 \times 4$ or better to sample the Brillouin zone of all structures. Atomic coordinations and the cell parameters were both relaxed until all the forces and components of the stress tensor are below 0.01 eV/Å and 0.2 kbar, respectively.

Phonons are calculated using the supercell force constant method (as implemented in the program described in refs^{26,27}). The vibrational frequencies (ω_i) of phonon modes can be calculated from the direct force-constant approach²⁸: the forces acting on atoms are generated by series of symmetry inequivalent atomic displacements about the equilibrium geometry, and fitted to cubic splines to extract the force constants. We used five displacements separated by 0.03Å, lying symmetrically around the equilibrium position. The lattice-dynamics calculations for all the structures were evaluated within the harmonic approximation^{29,30}. By constructing and diagonalizing the force dynamical matrix, the frequencies were extracted.²⁸ After extracting the phonon frequencies, we obtain finite-temperature thermodynamics by adding the vibrational contributions to the static electronic energies (equation 3). Within the harmonic approximation these contributions are given by equation 1 and 2, where ω_i is the normal-mode frequency and the sums run over all vibrational frequencies.

$$H_{vib}(T) = \sum_i \frac{1}{2} \hbar \omega_i + \hbar \omega_i \left[\exp \left(\frac{\hbar \omega_i}{k_B T} \right) - 1 \right]^{-1}, \quad (1)$$

$$S_{vib}(T) = k_B \sum_i \frac{\hbar \omega_i / k_B T}{\exp(\hbar \omega_i / k_B T) - 1} - \ln \left[1 - \exp \left(\frac{-\hbar \omega_i}{k_B T} \right) \right], \quad (2)$$

$$H(T) = E + H_{vib}(T) \quad (3)$$

$$G(T) = H(T) - TS(T). \quad (4)$$

Once the normal-mode frequencies have been determined, the zero-point energy (ZPE) can be recovered from equation 1 in the limit $H_{vib}(T=0\text{K})$.

B. Determining Hydrogen Desorption Reactions

We use the grand canonical linear programming (GCLP) method³¹ to determine the lowest-free-energy thermodynamic decomposition reactions pathways. GCLP is an automated method to determine the thermodynamically preferred reaction pathway, and has been applied to a wide range of hydrogen storage reactions^{32–35}, and more recently to determine lithiation pathways for Li-ion battery anodes^{36,37}. In our study, the following phases were considered: gas-phase H_2 and bulk solids B, Li, Zn, LiB, LiB_9 , LiB_{11} , LiH, LiZn, $LiBH_4$, $Li_2B_{12}H_{12}$, $Zn(BH_4)_2$ and $LiZn_2(BH_4)_5$.

III. RESULTS

A. Crystal Structures of $LiBH_4$, $Zn(BH_4)_2$, $LiZn(BH_4)_3$ and $LiZn_2(BH_4)_5$

We begin by discussing the crystal structures of the two single-metal borohydrides, and subsequently discuss the mixed Li Zn borohydrides. The crystal structure of $LiBH_4$ is well studied and exists in both low and high temperature forms. We found 12 entries for $LiBH_4$ in the Inorganic Crystal Structure Database (ICSD)⁴⁹, and calculated all of these available crystal structures of $LiBH_4$, to determine the one which possesses the lowest static DFT energy. With four BH_4 units tetrahedrally arranged around a Li atom, the structure of $LiBH_4$ with the lowest static DFT energy is orthorhombic with space group $Pnma$, which is in agreement with the observed low temperature (T=3.5K) phase⁴⁶. Upon DFT relaxation of the experimental crystal structure of $LiBH_4$, the lattice parameters, a, b, and c are 7.32, 4.38 and 6.58 Å, respectively, which are within 2.8% of experimental values (table I). Moreover, the DFT-relaxed $LiBH_4$ atomic positions are in fairly good agreement with the experimental data, and our calculations also support the recent theoretical study of Zhang *et al.*⁵⁰. Zhang *et al.* show that the experimentally observed $Pnma$ $LiBH_4$ structure is the lowest in energy in DFT.

In contrast to the $LiBH_4$ case, there is no well established crystal structure for $Zn(BH_4)_2$. Previous experimental and theoretical studies^{7,51} have tried to elucidate the $Zn(BH_4)_2$ structure. In order to identify a low-energy phase of $Zn(BH_4)_2$, we calculated DFT energies for $Zn(BH_4)_2$ in five known prototype crystal structures of chemically similar compounds with the same stoichiometry as $A(BC_4)_2$ in the database of ICSD. We found three low-energy structures are (indicated by their space groups): $F222$, $\bar{I}4m2$ with the $Mg(BH_4)_2$ prototype^{52,53}, and $I4_1cd$ with the $Be(BH_4)_2$ prototype⁵⁴. DFT static energies of these three structures are degenerate within 1 kJ/(mol BH_4). The next lowest-energy structure is $F2dd$ with $Ca(BH_4)_2$ prototype⁵⁵, which is 8 kJ/(mol BH_4) higher than the $F222$ structure (T=0K, static energy). In the following discussion, when we refer to $Zn(BH_4)_2$,

we use the $F222$ structure.

We next turn to the crystal structures of the mixed Li-Zn borohydrides. Compounds with $LiZn(BH_4)_3$ and $LiZn_2(BH_4)_5$ stoichiometries were proposed by previous theoretical and experimental reports, as described in the introduction^{13,14,16,18}. Utilizing DFT, we relax the two experimentally proposed structures (PXD and PND) for $LiZn_2(BH_4)_5$ (i.e. starting with the positions of the PXD or PND structure, and relaxing via DFT). The external cell parameters obtained upon DFT relaxing each of the two $LiZn_2(BH_4)_5$ experimental structures are summarized in table I as well as the structures of the other phases used in our subsequent discussion of reaction thermodynamics. The DFT relaxed structures are both orthorhombic ($Cmca$) but possess quite different lattice constants. The average absolute deviation (δ)⁵⁶ between theory and experiment for the lattice parameters is smaller for the structure determined from PND¹⁸, $\delta_{lattice}^{PND} = 1.4\%$, whereas for the structure determined from PXD¹⁴, $\delta_{lattice}^{PXD} = 3.4\%$. Compared to the structure determined by PND, the DFT relaxed result has similar lattice constants a and c ($\delta_a = 0.6\%$, $\delta_c = 1.0\%$), with a large discrepancy for b ($\delta_b = 2.6\%$). For each of the two DFT-relaxed structures, we compare the calculated internal atomic coordinates with the corresponding experimental values. We note the average absolute deviation of coordinates (δ)⁵⁶ between theory and experiment is smaller for the structure proposed by PND¹⁸, $\delta_{coord}^{PND} = 3.5\%$, whereas for the one proposed in PXD paper¹⁴, $\delta_{coord}^{PXD} = 8.0\%$. A comparison of the calculated and experimental bond lengths is also given in table II. The largest discrepancy between theory and experiment is in the bond length between Li and H atoms in the structure proposed by PXD (0.8 Å difference for Li-H12, as shown in table II). Overall, our DFT calculations clearly support the PND structure of Ref¹⁸ in terms of lattice parameters, atomic positions, and bond lengths.

B. Phonon Calculations of $LiBH_4$, $Zn(BH_4)_2$ and $LiZn_2(BH_4)_5$

We have performed DFT phonon calculations of $LiBH_4$, $Zn(BH_4)_2$, and $LiZn_2(BH_4)_5$. The phonon DOS for these compounds are shown in Figure 1. For $LiBH_4$, we find no soft-mode instabilities for the orthorhombic $LiBH_4$ phase ($Pnma$), which agrees with previous theoretical calculations^{50,57–59}. Our calculations indicate that the $Pnma$ phase $LiBH_4$ is (at least locally) stable at zero and finite temperature, which agrees with the experimental observation of Hartman *et al.*⁴⁶ that the observed low temperature (T=3.5K) phase is $Pnma$. The largest discrepancy between the X-ray and neutron experimental structures for $LiZn_2(BH_4)_5$ is the orientation of BH_4 group, which provides an interesting case to understand the trends in phonon and their effect on the thermodynamic stability as a function of structure. The two experimentally proposed $LiZn_2(BH_4)_5$ structures share the

TABLE I. DFT relaxed structural parameters for the phases in the Li-Zn-B-H system compared with experimental data. Bond lengths (d) and crystal lattice constants (a , b , c) are listed in Å, angles between lattice vectors are given in degrees. Crystal symmetry information is shown in parentheses. The experimental values obtained from literatures are listed in the reference column.

System	Parameter	Calculated	Experiment	Reference
H ₂ (gas)	d (H-H)	0.75	0.74	38
Li ($Fm\bar{3}m$)	a	4.34	4.39	39
B ($R\bar{3}m$)	a	5.05	5.06	40
	α	58.1	58.1	40
Zn ($P6_3/mmc$)	a	2.66	2.66	41
	c	4.98	4.91	41
LiH ($Fm\bar{3}m$)	a	4.02	4.07	42
LiB ($Pnma$)	a	6.19	6.40	43
	b	3.07	3.00	43
	c	5.71	5.60	43
LiB ₉ ($P6_3cm$)	a	5.74	5.65	44
	c	5.03	5.04	44
LiB ₁₁ ($R\bar{3}m$)	a	4.82	4.98	45
	c	12.99	11.12	45
LiBH ₄ ($Pnma$)	a	7.32	7.12	46
	b	4.38	4.40	46
	c	6.59	6.67	46
Li ₂ B ₁₂ H ₁₂ ($Pa\bar{3}$)	a	9.60	9.58	47
LiZn ($Fd\bar{3}m$)	a	6.15	6.23	48
Zn(BH ₄) ₂ ($F222$)	a	9.53	—	—
	b	9.95	—	—
	c	12.28	—	—
LiZn ₂ (BH ₄) ₅ ($Cmca$)	a	8.43	8.62	14
(PXD)	b	19.07	17.90	14
	c	15.19	15.41	14
LiZn ₂ (BH ₄) ₅ ($Cmca$)	a	8.55	8.60	18
(PND)	b	18.36	17.89	18
	c	15.21	15.36	18

similar Li and Zn positions, which form an interpenetrated three-dimensional framework. The BH₄ groups, bridging the two Zn atoms, have the same orientation in both structures. However, the BH₄ group, bridging the Zn and Li atoms, have a 180° discrepancy. The configuration of BH₄ orientation makes the PND structure more “close-packed” than the PXD structure.

From our DFT phonon calculations of LiZn₂(BH₄)₅ in both the PXD and PND structures, we find the PXD structure has a strong instability with a maximum imaginary frequency of $173i$ cm⁻¹. However, the DFT phonon calculations of the PND structure of LiZn₂(BH₄)₅ *does not yield* any imaginary modes. The phonon calculations strongly support the validity and stability of PND structure at zero and low temperatures. Figure 1 shows the phonon DOS of LiBH₄, Zn(BH₄)₂ and [LiZn₂(BH₄)₅]_{PND} (i.e. PND structure, but DFT-relaxed). The DOS of [LiZn₂(BH₄)₅]_{PND} has similar behavior of the DOS of LiBH₄ and Zn(BH₄)₂, with metal ions (Li⁺, Zn²⁺) mainly contributing at low frequencies (<500 cm⁻¹), and boron hydrogen interaction at high frequencies (1000 cm⁻¹ ~ 2500 cm⁻¹). In the region of 1000 cm⁻¹ ~ 1500 cm⁻¹, we find phonons that involve bending of H-B-H

bond angles within the BH₄ tetrahedra, while at the highest frequencies 2000 cm⁻¹ ~ 2500 cm⁻¹, we find phonons that stretch elastically stiff B-H bonds.

C. Phase Stability of LiZn₂(BH₄)₅

We next consider the stability of the mixed Li-Zn borohydrides relative to the energies of the other mixed borohydrides as well as the individual single-metal borohydrides, i.e. LiBH₄ and Zn(BH₄)₂. Specifically we examine the stability of three mixed compounds: the LiZn₂(BH₄)₅ compound in both the PXD and PND structures, and the theoretically proposed LiZn(BH₄)₃ compound¹⁶. The phase stability is determined by the mixing energy, which is given by:

$$\Delta G = G_{\text{Li}_x\text{Zn}_{(1-x)}(\text{BH}_4)_{(2-x)}} - xG_{\text{LiBH}_4} - (1-x)G_{\text{Zn}(\text{BH}_4)_2}, \quad (5)$$

where the free energy G of each phase is given by equation 4, determined from the combination of DFT T=0K static total energy $E_{\text{tot}}(T=0\text{K})$, the zero-point energy E_{ZPE} , and the enthalpic + entropic vibrational contributions ($H_{\text{vib}} - TS_{\text{vib}}$). So for each phase, $G = E_{\text{tot}}(T=0\text{K})$

TABLE II. Comparison of calculated interatomic distances with values determined from PXD (Ref.¹⁴) and PND (Ref.¹⁸) studies. In each case of the ‘‘DFT’’ column, we started with the structures and positions of the experimental values and relaxed within DFT. Lengths are given in Å. 2× indicates that there are two H (or B) ions having the identical bond length with the metal Li (or Zn) ion.

Parameter		DFT	Experiment(PXD) ¹⁴		DFT	Experiment(PND) ¹⁸
Zn1-H13	2×	1.835	1.788	2×	1.843	1.833
Zn1-H21		1.849	1.698			
Zn1-H22		1.899	1.831			
Zn1-H23				2×	1.840	1.799
Zn1-H33	2×	1.964	1.830	2×	1.943	1.835
Zn2-H31		1.958	2.132		1.961	1.96(3)
Zn2-H32		1.939	1.683		1.945	1.81(3)
Zn2-H43	2×	1.835	1.652	2×	1.833	1.79(2)
Zn2-H41	2×	1.850	1.916	2×	1.854	1.91(2)
Average		1.88	1.81		1.88	1.84
Zn1-B1		2.181	2.108		2.178	2.168
Zn1-B2		2.194	2.164		2.183	2.201
Zn1-B3		2.294	2.203		2.266	2.238
Zn2-B3		2.268	2.312		2.270	2.20(2)
Zn2-B4	2×	2.181	2.125	2×	2.182	2.204
Average		2.22	2.17		2.21	2.20
Li1-H11		2.093	2.00(3)		2.139	2.13(10)
Li1-H12		2.112	2.91(4)		2.139	2.64(11)
Li1-H21					2.088	2.05(10)
Li1-H22					2.062	1.98(10)
Li1-H23	2×	2.140	1.96(3)			
Li1-H42	2×	2.188	2.20(3)	2×	2.107	1.88(7)
Li1-H44	2×	2.132	1.931	2×	2.134	2.22(4)
Average		2.14	2.14		2.11	2.13
Li1-B1		2.494	2.89(3)		2.444	2.80(10)
Li1-B2		2.514	2.36(3)		2.463	2.41(9)
Li1-B4	2×	2.446	2.473	2×	2.472	2.39(2)
Average		2.48	2.55		2.46	2.50

+ $E_{\text{ZPE}} + H_{\text{vib}} - TS_{\text{vib}}$, is given by a combination at DFT static, relaxed total energies and phonon calculations. To clarify the following discussion, we label the PEGS+DFT predicted $\text{LiZn}(\text{BH}_4)_3$ structure as $[\text{LiZn}(\text{BH}_4)_3]_{\text{PEGS}}^{16}$, and the X-ray $\text{LiZn}_2(\text{BH}_4)_5$ structure as $[\text{LiZn}_2(\text{BH}_4)_5]_{\text{PXD}}^{14}$, and the PND structure as $[\text{LiZn}_2(\text{BH}_4)_5]_{\text{PND}}^{18}$. But we reiterate that in all cases, we relax these initial geometries within DFT to their minimum energy geometries. Including only the static DFT energy (and no ZPE), we refer to the analogous energy difference as $\Delta E_{\text{mix}}^{T=0K}$. Our DFT calculations of $[\text{LiZn}(\text{BH}_4)_3]_{\text{PEGS}}^{16}$, give a mixing energy $\Delta E_{\text{mix}}^{T=0K} = -7.6$ kJ/(mol cation), indicating the stability with respect to the decomposition into the single metal borohydrides (figure 2), i.e. LiBH_4 and $\text{Zn}(\text{BH}_4)_2$. This result is in agreement with the previous calculations of Aidhy *et al.*¹⁶. The $[\text{LiZn}_2(\text{BH}_4)_5]_{\text{PXD}}$ structure proposed by PXD has a $\Delta E_{\text{mix}}^{T=0K} = -3.2$ kJ/(mol cation) mixing energy and is also plotted in figure 2. Regarding this $[\text{LiZn}_2(\text{BH}_4)_5]_{\text{PXD}}$ compound, our calculations

agree with what Aidhy *et al.* have found¹⁶: the relative small mixing energy makes $[\text{LiZn}_2(\text{BH}_4)_5]_{\text{PXD}}$ lie above the tie line between $[\text{LiZn}(\text{BH}_4)_3]_{\text{PEGS}}$ and $\text{Zn}(\text{BH}_4)_2$, showing that the structure proposed by PXD is not a stable ground state at $T=0\text{K}$. However, we find the mixing energy for the $[\text{LiZn}_2(\text{BH}_4)_5]_{\text{PND}}$ structure is $\Delta E_{\text{mix}}^{T=0K} = -11$ kJ/(mol cation), which is lower than the mixing free energy of $[\text{LiZn}_2(\text{BH}_4)_5]_{\text{PXD}}$, indicating the stability and validity of the PND structure of $\text{LiZn}_2(\text{BH}_4)_5$. As shown in figure 2, the PEGS+DFT predicted $[\text{LiZn}(\text{BH}_4)_3]_{\text{PEGS}}$ structure is found to lie *above* the tie line between $[\text{LiZn}_2(\text{BH}_4)_5]_{\text{PND}}$ and $\text{Zn}(\text{BH}_4)_2$ (with or without including the vibrational contribution). Therefore, we conclude that the $[\text{LiZn}_2(\text{BH}_4)_5]_{\text{PND}}$ phase is a stable ground state in the mixed Li Zn borohydrides system, and the previously proposed $[\text{LiZn}(\text{BH}_4)_3]_{\text{PEGS}}$ structure is not a $T=0\text{K}$ stable ground state. Our conclusion appears to contradict the work of Aidhy *et al.*¹⁶, where they found the $[\text{LiZn}(\text{BH}_4)_3]_{\text{PEGS}}$ is the ground state, simply because, at that time, the correct, low-energy struc-

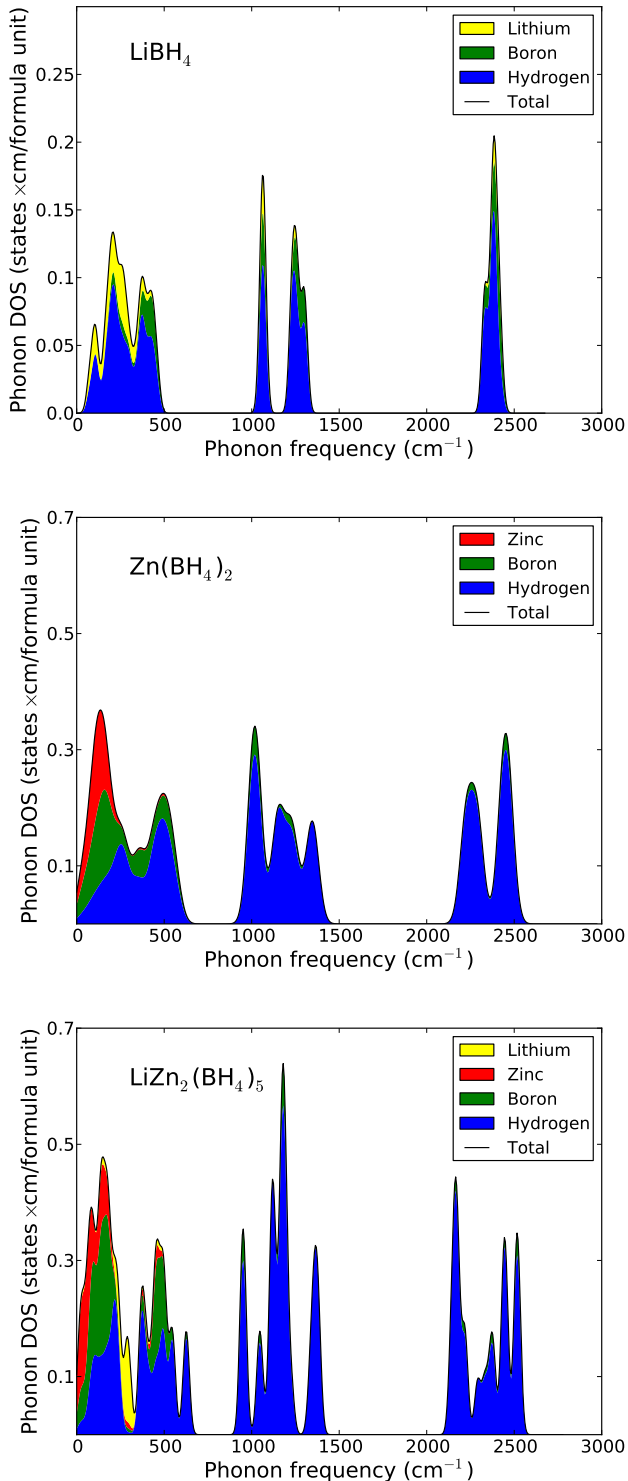


FIG. 1. (Color online) Calculated phonon DOS of LiBH_4 , $\text{Zn}(\text{BH}_4)_2$ and $\text{LiZn}_2(\text{BH}_4)_5$. The structure information of $\text{LiZn}_2(\text{BH}_4)_5$ is obtained from DFT relaxed powder neutron diffraction determined structure¹⁸. (Please note that the pDOS of $\text{LiZn}_2(\text{BH}_4)_5$ are 0 at frequency 0. In the figure, there appears to be a finite contribution at zero frequency, which is merely due to the broadening width of phonon modes used to construct the DOS.)

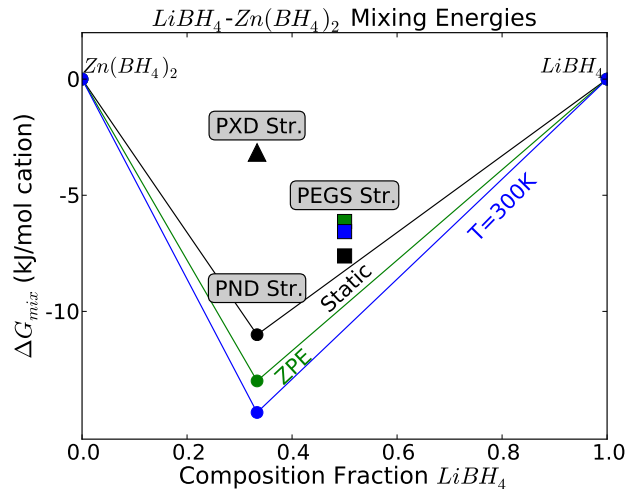


FIG. 2. Mixing Energy (with and without considering vibrational contribution) vs composition plot for systems involving LiBH_4 and $\text{Zn}(\text{BH}_4)_2$. The two experimental structures (Refs.¹⁴ and¹⁸) are labeled as PXD Str. and PND Str., and PEGS Str. is the structure from theoretical PEGS+DFT prediction¹⁶. The black line and dots indicate the convex hull and mixing energies from the static calculation results, while the green and blue are for ZPE and $T=300\text{K}$ respectively. $\text{LiZn}(\text{BH}_4)_3$ (Ref¹⁶) is found to lie above the tie line between $\text{LiZn}_2(\text{BH}_4)_5 + \text{Li}(\text{BH}_4)_2$, indicating that $\text{LiZn}(\text{BH}_4)_3$ is not a stable ground state in this system. PND Str. lies on the convex hull, indicating that it is a stable ground state in this system.

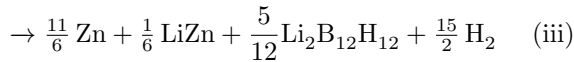
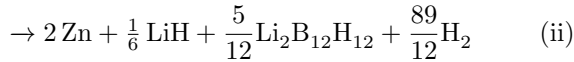
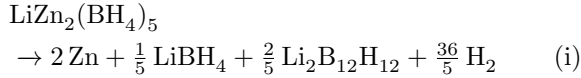
ture of $[\text{LiZn}_2(\text{BH}_4)_5]_{\text{PND}}$ has not been proposed. This recently suggested $[\text{LiZn}_2(\text{BH}_4)_5]_{\text{PND}}$ structure¹⁸ completely changes the ground state phase stability in the Li-Zn-BH₄ system, as shown in figure (2), and brings the calculated DFT borohydride stability in agreement with experiment: $\text{LiZn}_2(\text{BH}_4)_5$ is stable with respect to decomposition into other borohydrides, but $\text{LiZn}(\text{BH}_4)_3$ is not.

D. Energetics and thermodynamics of $\text{LiZn}_2(\text{BH}_4)_5$ decomposition

Having discussed the crystal structure and phase stability of $\text{LiZn}_2(\text{BH}_4)_5$, we next turn to evaluate the energetics of decomposition in the lithium zinc borohydride system. We begin with the static energetics and subsequently discuss the effects of zero-point energies, vibrational entropies and the gas phase hydrogen dynamical contributions. To examine the finite-temperature thermodynamics of the decomposition reactions, we need to obtain the total energies of all possible reactant and product phases in the Li-Zn-B-H system. A summary of the compounds used, their crystal structures, and a comparison of the calculated structures to experimental data are presented in table I. Armed with these DFT energies of metals, hydrides, borides and borohydrides, we

use the Grand Canonical Linear Programming method (GCLP)³¹ to identify all the thermodynamically favored reactions in the quaternary Li-Zn-B-H system.

We first consider the GCLP calculations of $\text{LiZn}_2(\text{BH}_4)_5$ decomposition. Using the static $T=0\text{K}$ DFT energies (i.e. not ZPE-corrected) in GCLP, we identify the lowest energy thermodynamic decomposition pathway. We find that the thermodynamic decomposition path for $\text{LiZn}_2(\text{BH}_4)_5$ involves four reaction steps:



The first reaction step (i) involves the weakly exothermic decomposition [$\Delta E_{static}^{T=0K} = -1.3 \text{ kJ}/(\text{mol H}_2)$] of $\text{LiZn}_2(\text{BH}_4)_5$, indicating that this compound is not thermodynamically stable at $T=0\text{K}$. The instability of this compound follows from the fact that $\text{Zn}(\text{BH}_4)_2$ itself is only weakly stable with respect to the decomposition into $\text{Zn} + 2 \text{B} + 4 \text{H}_2$. Based on our calculation, $\text{Zn}(\text{BH}_4)_2$ has a slightly endothermic decomposition enthalpy at room temperature, $\Delta H^{T=300K} = +2.8 \text{ kJ}/(\text{mol H}_2)$ and $\Delta H_{ZPE}^{T=0K} = -2.9 \text{ kJ}/(\text{mol H}_2)$. Compared to this, hydrogen release from the $\text{LiZn}_2(\text{BH}_4)_5$ compound is changed by two competing effects: 1) $\text{LiZn}_2(\text{BH}_4)_5$ is *stabilized* by the fact that it is bound in the mixed borohydride with a mixing energy of $-11 \text{ kJ}/(\text{mol H}_2)$ (figure 2); 2) however, this effect is more than compensated by the *destabilization* due to the fact that B in the product phases of reaction (i) is not pure B (as in the decomposition of $\text{Zn}(\text{BH}_4)_2$), but rather is in strongly bound $\text{LiBH}_4 + \text{Li}_2\text{B}_{12}\text{H}_{12}$ compounds. The second reaction (ii) is endothermic [$\Delta E_{static}^{T=0K} = +60.9 \text{ kJ}/(\text{mol H}_2)$] and essentially involves the decomposition of $\text{LiBH}_4 \rightarrow \frac{1}{12} \text{Li}_2\text{B}_{12}\text{H}_{12} + \frac{5}{6} \text{LiH} + \frac{13}{12} \text{H}_2$. The third reaction (iii) is endothermic and involves the combination of $\text{LiH} + \text{Zn} \rightarrow \text{LiZn} + \frac{1}{2} \text{H}_2$. This reaction is a classic example of destabilizing a strongly bound hydride (LiH) by combining with a reactant (Zn) that will form a strongly bound product (LiZn). Examples of this include $\text{MgH}_2 + \text{Si}$, $\text{LiBH}_4 + \text{MgH}_2$, $\text{LiBH}_4 + \text{MH}_x$ and others⁶⁰. The final step (iv) involves a complicated, multi-phase reaction, $2 \text{Zn} + \text{Li}_2\text{B}_{12}\text{H}_{12} \rightarrow 2 \text{LiZn} + 12 \text{B} + 6 \text{H}_2$, which is highly endothermic. In figure 3, we present the energetics for these four reaction steps. We note from Fig 3 that with our lowest-energy predicted phases, all five stoichiometries lie on a convex hull. The reaction enthalpies (per mol H_2) are given by the slopes of the lines connecting reactants and products. In this graphical interpretation, the convex hull requires that the slopes must get increasingly positive as more H_2 is released. That is, the energetics of decomposition must become monotonically

more endothermic as the decomposition proceeds.

For all phases involved in the reactions predicted by GCLP, we also calculated the zero-point energy (ZPE) contributions (table III). We compute the zero-point contributions from DFT phonon calculations. We compare our calculations of ZPE for several phases with previous DFT calculations in table III, showing good agreement. With these vibrational contributions, we see that the zero-point energies (ZPE) decrease the static reaction enthalpies by about $17\text{-}24 \text{ kJ}/(\text{mol H}_2)$ (as shown in table IV), with exception for reaction (3) $\text{Zn} + \text{LiH} \rightarrow \text{LiZn} + \frac{1}{2} \text{H}_2$ [reaction enthalpy decreases $4.5 \text{ kJ}/(\text{mol H}_2)$]. The contribution of ZPE to reaction enthalpies can be explained in terms of the differences between metal and non-metal atom vibrations. The metal cations in hydrides and borohydrides contribute mainly to the librational vibrations whose frequencies are considerably lower than those involving H (e.g. H_2 vibrations, metal-H vibrations, or the internal B-H bending and stretching modes of BH_4^- or $\text{B}_{12}\text{H}_{12}^{2-}$ anions). As shown in figure 1, the frequencies of metal cations are constrained in the range of $0\sim 500 \text{ cm}^{-1}$, while the B-H vibrational modes can readily reach 2000 cm^{-1} . The phonon frequencies of the bulk metal and alloy are also expected to be low. Hence, the ZPE contributions to ΔH are qualitatively determined by the difference in the proportion of “high-frequency” vibrational modes between reactants and products. In reaction $\text{Zn} + \text{LiH} \rightarrow \text{LiZn} + \frac{1}{2} \text{H}_2$, the “low frequency” ZPE contributions of bulk zinc largely cancels out that of LiZn, and “high frequency” contributions of H_2 and LiH also partly cancel, which results in the ZPE contribution to reaction (3) being smaller than the other three reactions in table IV. Although, ZPE contributions are different for the four reactions in table IV, including ZPE still maintains the order of monotonically more endothermic reactions as H_2 is released. That indicates the decomposition pathway shown in figure 3 is still on a convex hull after including ZPE. We also include the finite-temperature enthalpic contributions, specifically at $T=300\text{K}$. Apart from the vibrational contributions of crystal phases at $T=300\text{K}$, an additional H_2 gas enthalpy term is added to equation 1, due to the translational ($\frac{3}{2}RT$), rotational (RT), and pV degrees (RT) of freedom ($\frac{7}{2}RT$ in total). The enthalpies of $T=300\text{K}$ are shown in table IV. Our $T=300\text{K}$ enthalpies result in the same decomposition pathway as $T=0\text{K}$, which indicates that after including the enthalpy of H_2 and vibrational contributions, the decomposition enthalpies as shown in figure 3 are still on a convex hull.

The critical temperature in table IV is derived from the Van’t Hoff equation,

$$\ln(p) = (-\Delta H/RT) + (\Delta S/R), \quad (6)$$

where T_c is obtained by setting the H_2 pressure at 1 bar in equation 6. To utilize Van’t Hoff equation, we need to know the reaction enthalpy and entropy. The enthalpies of crystal phases can be determined by equation 3, while for the linear molecules, i.e., hydrogen gas, in addition

TABLE III. Calculated vibrational contributions (at T=300K) to the free energies of phases used in this study. ZPE refers to the zero-point energy, given by $H_{vib}(T=0K)$ (equation 1); $E_{vib}^{300K} = H_{vib}(T = 300K) - ZPE$; S_{vib} is the vibrational entropy. Units are kJ/(mol f.u.) for ZPE and E_{vib} , and J/(mol K f.u.) for S_{vib} .

System	ZPE	ZPE (previous DFT)	Reference	$E_{vib}^{T=300K}$	$S_{vib}^{T=300K}$
H ₂	25.9	26.3	⁶¹	≈ 0	≈ 0
		25.7, 26.1	⁵⁷ and ⁵⁸		
B	13.4	12.2	⁵⁸	0.9	4.0
Li	3.5	3.9	⁵⁸	4.6	29.3
Zn	1.6			6.0	48.7
LiH	22.2	21.4, 21.8	⁵⁸ and ⁶²	3.3	16.6
LiB	15.9			5.8	34.0
LiB ₉	113.9			14.5	70.1
LiB ₁₁	129.3			19.7	99.3
LiBH ₄	110.4	108.1	⁵⁹	11.1	65.5
		103.0, 106.5	⁵⁸ and ⁵⁷		
Li ₂ B ₁₂ H ₁₂	455.3			32.9	197.6
LiZn	8.5			8.4	54.4
Zn(BH ₄) ₂	207.9			20.1	133.6
LiZn ₂ (BH ₄) ₅ ¹⁸	520.8			52.0	349.0

TABLE IV. The energetics of decomposition in the LiZn₂(BH₄)₅ system. $\Delta E_{static}^{T=0K}$ is the static energetics. The effects of zero-point energies (ZPE) are also indicated by $\Delta H_{ZPE}^{T=0K}$. The full dynamic calculations at T=300K, which include the contributions from the vibrational energies as well as the enthalpy of H₂ gas, are listed in the $\Delta H^{T=300K}$ column, followed by the entropy contribution (ΔS^{300K}) due to vibrational entropies and the entropy of H₂ gas. The units of enthalpies and entropies are in kJ/(mol H₂) and J/(K mol H₂), respectively. Applying the van's Hoff equation ($\ln p = -\Delta H/RT + \Delta S/R$), we can predict the critical temperatures (T_c) at $p = 1$ bar H₂ pressure, and the unit of T_c is in degree Celsius ($^{\circ}C$).

Reaction	$\Delta E_{static}^{T=0K}$	$\Delta H_{ZPE}^{T=0K}$	$\Delta H^{T=300K}$	$\Delta S^{T=300K}$	T_c
(1) LiZn ₂ (BH ₄) ₅ → 2 Zn + $\frac{1}{5}$ LiBH ₄ + $\frac{2}{5}$ Li ₂ B ₁₂ H ₁₂ + $\frac{36}{5}$ H ₂	-1.3	-19.0	-13.6	108.7	
(2) 12 LiBH ₄ → 10 LiH + Li ₂ B ₁₂ H ₁₂ + 13 H ₂	60.9	36.9	40.5	98.4	138
(3) Zn + LiH → LiZn + $\frac{1}{2}$ H ₂	78.1	73.6	80.4	109.1	453
(4) 2 Zn + Li ₂ B ₁₂ H ₁₂ → 2 LiZn + 12 B + 6 H ₂	125.9	104.9	110.7	107.8	754

to the vibrational enthalpy added to the static electronic energies, translational, rotational enthalpies and pV term ($\frac{5}{2}RT + pV = \frac{7}{2}RT$) contributions should be taken into account. The vibrational entropies of crystal phases are determined by equation 2, and the entropy for gas-phase hydrogen is given by:

$$S_{H_2} = R \left(\frac{7 \ln(T)}{2} - \ln(p) - 4.222 \right) \quad (7)$$

where the constant -4.222 is the fitting parameter with respect to the experimental values⁶³. The reaction entropy ΔS is dominated by the entropy of H₂ gas [$S_{H_2} = 130.9$ J/(K mol H₂) at T=300K and p=1 bar], however, the vibrational entropies of the crystalline phases shift ΔS by 22~33 J/(K mol H₂) (table IV). If one ignores the entropies of the crystalline phases, the target window of $T_{dehydrogenation} \leq 80^{\circ}C$, $P_{rehydrogenation} \leq 700$ bar set by the operating temperature of proton exchange membrane fuel cells and pressure limits of current tanks will result in a range of $\Delta H \approx 20 - 50$ kJ/(mol H₂) for the reaction enthalpy⁶⁴. This range appears to include the

decomposition of LiBH₄ (table IV). However, after including the entropy contributions from crystalline phases, the T_c for LiBH₄ is 138 $^{\circ}C$, higher than the target range. Therefore, the vibrational entropy can play an important role in a quantitatively accurate calculation of the thermodynamics of H₂ decomposition reactions. According to the Van't Hoff equation, there is a linear relationship between $\ln(p)$ and $1/T$, where the slope is determined by the reaction enthalpy and the intercept is obtained by the reaction entropy. Figure 4 shows these relations (the so-called van't Hoff diagrams) for the decomposition reactions of LiZn₂(BH₄)₅ from table IV. Figure 4 shows, unfortunately, that *there is no near-ambient thermodynamically reversible hydrogen storage reaction in the Li-Zn-B-H system*.

Our calculations of the energetics of LiZn₂(BH₄)₅ decomposition are consistent with recent experimental results, in which, Borgschulte *et al*⁶⁵ found LiZn₂(BH₄)₅ decomposes according to the pathway LiZn₂(BH₄)₅ → 2 Zn(BH₄)₂ + LiBH₄. Moreover, Ravnsbæk *et al*¹⁴ found LiZn₂(BH₄)₅ decomposes slowly at

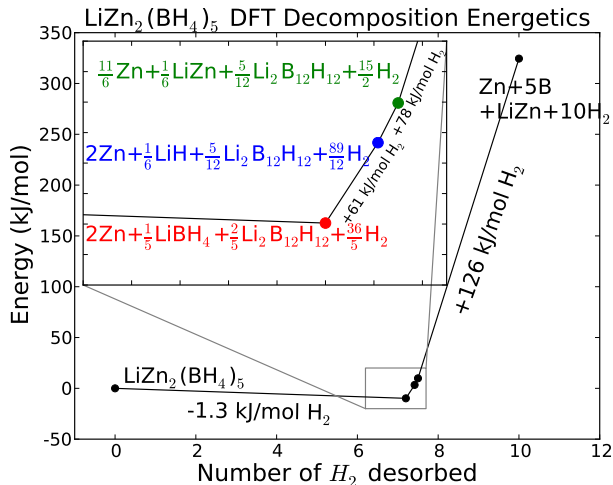


FIG. 3. DFT-predicted static energetics decomposition paths of $\text{LiZn}_2(\text{BH}_4)_5$. The energetics are shown for five distinct hydrogen contents, corresponding to stoichiometries $\text{LiZn}_2(\text{BH}_4)_5$, LiBH_4 , LiH , $\text{Li}_2\text{B}_{12}\text{H}_{12}$ and LiZn . Since the plot is the sum of the energies of the coexisting phases versus the number of desorbed H_2 molecules at each stoichiometry, the decomposition energies (per mol H_2) are simply the slopes of the lines connecting the points. The effects of zero-point energies, vibrational entropies, and dynamical contributions to the H_2 equation of state are included in Table IV and discussed in the text.

room temperature when stored in argon atmosphere, and metallic zinc formed after approximately one week. This experimental observation consists with our theoretical predictions: (i) we found, at $T=300\text{K}$, the decomposition enthalpy for $\text{LiZn}_2(\text{BH}_4)_5$ is $-13.6 \text{ kJ}/(\text{mol } \text{H}_2)$ (table IV), and the slight exothermic enthalpy indicates $\text{LiZn}_2(\text{BH}_4)_5$ is unstable at room temperature; (ii) we predicted metallic zinc is one of the products. Based on our calculations, the decomposition enthalpy of $\text{LiZn}_2(\text{BH}_4)_5$ is far smaller than that of LiBH_4 , but in the same magnitude of $\text{Zn}(\text{BH}_4)_2$ (as shown in table IV).

E. The thermodynamics of B_2H_6 release from borohydride decomposition

In our GCLP calculations, we did not take release of gas-phase B_2H_6 into account, which is often observed as an important but unwanted by-product in dehydrogenation. Because the formation of diborane ($2\text{B} + 3\text{H}_2 \rightarrow \text{B}_2\text{H}_6$) is endothermic, $\Delta H_{\text{form}}^{T=0\text{K}} = +56.7 \text{ kJ}/(\text{mol } \text{B}_2\text{H}_6)$ and $\Delta H_{\text{form}}^{T=300\text{K}} = +41.0 \text{ kJ}/(\text{mol } \text{B}_2\text{H}_6)$ (experimental values from reference⁶³), it is not thermodynamically stable, and will not be present in the thermodynamically-preferred reaction pathway. (In other words, release of H_2 will always be thermodynamically favored over diborane release, as long as $2\text{B} + 3\text{H}_2$ has a lower free energy than B_2H_6 .) However, despite

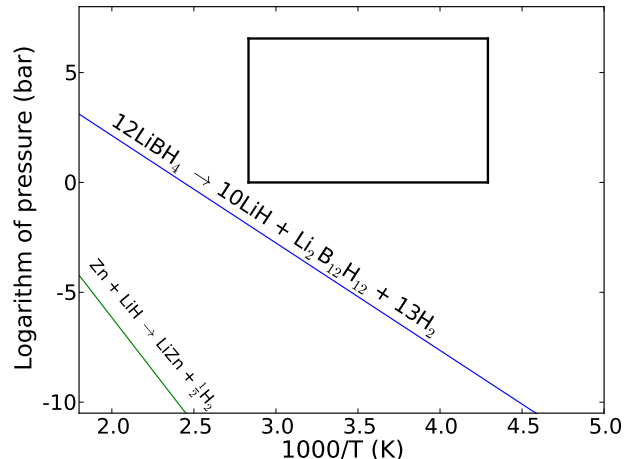


FIG. 4. Calculated van't Hoff plot for reactions listed in Table IV. The region within the rectangular box corresponds to desirable temperatures and pressures for on-board hydrogen storage: $p_{\text{H}_2} = 1 \sim 700 \text{ bar}$ and $T = -40 \sim 80^\circ\text{C}$. Since reaction (4) in Table IV far away the target window, we only indicate the reaction (2) and (3) in the figure.

its thermodynamic instability, diborane can be released during dehydrogenation, especially in cases where hydrogen release is kinetically hindered. In recent experimental work, Borgschulte *et al*⁶⁵ found the $\text{LiZn}_2(\text{BH}_4)_5$ decomposition pathway as $\text{LiZn}_2(\text{BH}_4)_5 \rightarrow 2\text{Zn}(\text{BH}_4)_2 + \text{LiBH}_4 \rightarrow 2\text{B}_2\text{H}_6 + 2\text{H}_2 + 2\text{Zn} + \text{LiBH}_4 \rightarrow 2\text{B}_2\text{H}_6 + \frac{7}{2}\text{H}_2 + 2\text{Zn} + \text{LiH} + \text{B}$. Although our GCLP calculations will not predict the existence of B_2H_6 , due to its thermodynamic instability, our results for the decomposition pathway are qualitatively consistent with Borgschulte *et al*⁶⁵: the “weak” part $[\text{Zn}(\text{BH}_4)_2]$ of the mixed borohydride decomposes first, leaving the “strong” part (LiBH_4) to react subsequently.

IV. CONCLUSIONS

Single metal borohydrides often do not have ideal thermodynamic properties, but rather are either too weakly bound or too strongly bound. We address the problem of finding mixed metal borohydrides with favorable thermodynamics and illustrate the approach using the example of $\text{LiZn}_2(\text{BH}_4)_5$. Combined with the grand canonical linear programming method (GCLP), we employed density functional theory (DFT) calculations to study the experimentally and computationally proposed crystal structures and the finite-temperature formation and dehydrogenation thermodynamics for the quaternary hydride $\text{LiZn}_2(\text{BH}_4)_5$. Our DFT and frozen phonon calculations suggest that the experimental PND study¹⁸ yields a $\text{LiZn}_2(\text{BH}_4)_5$ crystal structure with DFT energy lower than the one determined from PXD¹⁴. Our DFT calculations show that when using the neutron-diffraction struc-

ture of $\text{LiZn}_2(\text{BH}_4)_5$, the recently theoretically predicted $\text{LiZn}(\text{BH}_4)_3$ compound¹⁶ is unstable with respect to the decomposition into $\text{LiZn}_2(\text{BH}_4)_5 + \text{LiBH}_4$. For reaction energetics, we utilized the GCLP method and predicted the thermodynamically stable decomposition pathway of $\text{LiZn}_2(\text{BH}_4)_5$. We found that the weakly bound portion $[\text{Zn}(\text{BH}_4)_2]$ in $\text{LiZn}_2(\text{BH}_4)_5$ decomposes first at low temperature, leaving the strongly bound portion (LiBH_4). As the temperature increases, the strongly bound portion (LiBH_4) consequently decomposes. In our identified reaction pathway, the decomposition of $\text{LiZn}_2(\text{BH}_4)_5$ consists of four reaction steps: the first is slightly exothermic [$\Delta E_{static}^{T=0K} = -1.3 \text{ kJ}/(\text{mol H}_2)$], followed by three strong endothermic reaction steps. Unfortunately, none of critical temperatures of these reactions falls in the range of near ambient reversible storage. The behavior of $\text{LiZn}_2(\text{BH}_4)_5$ shows that mixed metal borohydrides formed by mixing borohydrides of high and low thermodynamics stabilities do not necessarily have an intermediate decomposition tendency. Our results suggest the correct strategy to find intermediate decomposition in mixed metal borohydrides is to search for stable mixed-metal products such as ternary metal borides.

ACKNOWLEDGMENTS

Y.W. and C.W. gratefully acknowledge financial support from the US Department of Energy under Grant Nos. DE-FC36-08GO18136. Y.Z. and C.W. gratefully acknowledge financial support from the US Department of Energy under Grant Nos. DE-FG02-07ER46433.

- ¹ Y. Nakamori, K. Miwa, A. Ninomiya, H. Li, N. Ohba, S.-i. Towata, A. Züttel, and S.-i. Orimo, *Phys. Rev. B* **74**, 045126 (2006).
- ² J. Yang, A. Sudik, C. Wolverton, and D. J. Siegel, *Chem. Soc. Rev.* **39**, 656 (2010).
- ³ D. J. Siegel, C. Wolverton, and V. Ozoliņš, *Phys. Rev. B* **76**, 134102 (2007).
- ⁴ N. Ohba, K. Miwa, M. Aoki, T. Noritake, S.-i. Towata, Y. Nakamori, S.-i. Orimo, and A. Züttel, *Phys. Rev. B* **74**, 075110 (2006).
- ⁵ Y. Filinchuk, D. Chernyshov, and R. Černý, *The Journal of Physical Chemistry C* **112**, 10579 (2008), <http://pubs.acs.org/doi/pdf/10.1021/jp8025623>.
- ⁶ N. A. Zarkevich and D. D. Johnson, *Phys. Rev. Lett.* **100**, 040602 (2008).
- ⁷ E. Jeon and Y. Cho, *Journal of Alloys and Compounds* **422**, 273 (2006).
- ⁸ W. Grochala and P. P. Edwards, *Chemical Reviews* **104**, 1283 (2004), <http://pubs.acs.org/doi/pdf/10.1021/cr030691s>.
- ⁹ K. Miwa, N. Ohba, S. Towata, Y. Nakamori, and S. Orimo, *Journal of Alloys and Compounds* **404-406**, 140 (2005).
- ¹⁰ H.-W. Li, S. Orimo, Y. Nakamori, K. Miwa, N. Ohba, S. Towata, and A. Züttel, *Journal of Alloys and Compounds* **446-447**, 315 (2007).
- ¹¹ Y. Nakamori and S. Orimo, *Journal of Alloys and Compounds* **370**, 271 (2004).
- ¹² R. Černý, N. Penin, V. D'Anna, H. Hagemann, E. Durand, and J. Růžička, *Acta Materialia* **59**, 5171 (2011).
- ¹³ J. S. Hummelshøj, D. D. Landis, J. Voss, T. Jiang, A. Tekin, N. Bork, M. Dulak, J. J. Mortensen, L. Adamska, J. Andersin, J. D. Baran, G. D. Barmparis, F. Bell, A. L. Bezanilla, J. Bjork, M. E. Bjorketun, F. Bleken, F. Buchter, M. Burkle, P. D. Burton, B. B. Buus, A. Calborean, F. Calle-Vallejo, S. Casolo, B. D. Chandler, D. H. Chi, I. Czekaj, S. Datta, A. Datye, A. DeLaRiva, V. Despoja, S. Dobrin, M. Engelund, L. Ferrighi, P. Frondelius, Q. Fu, A. Fuentes, J. Furst, A. Garcia-Fuente, J. Gavnholt, R. Goeke, S. Gudmundsdottir, K. D. Hammond, H. A. Hansen, D. Hibbitts, J. E. Hobi, J. G. Howalt, S. L. Hruby, A. Huth, L. Isaeva, J. Jelic, I. J. T. Jensen, K. A. Kacprzak, A. Kelkkanen, D. Kelsey, D. S. Kesanakurthi, J. Kleis, P. J. Klupfel, I. Konstantinov, R. Korytar, P. Koskinen, C. Krishna, E. Kunkes, A. H. Larsen, J. M. G. Lastra, H. Lin, O. Lopez-Acevedo, M. Mantega, J. I. Martinez, I. N. Mesa, D. J. Mowbray, J. S. G. Myrdal, Y. Natanzon, A. Nistor, T. Olsen, H. Park, L. S. Pedroza, V. Petzold, C. Plaisance, J. A. Rasmussen, H. Ren, M. Rizzi, A. S. Ronco, C. Rostgaard, S. Saadi, L. A. Salguero, E. J. G. Santos, A. L. Schoenhalz, J. Shen, M. Smedemand, O. J. Stausholm-Moller, M. Stibius, M. Strange, H. B. Su, B. Temel, A. Toftelund, V. Tripkovic, M. Vanin, V. Viswanathan, A. Vojvodic, S. Wang, J. Wellendorff, K. S. Thygesen, J. Rossmeisl, T. Bligaard, K. W. Jacobsen, J. K. Nørskov, and T. Vegge, *The Journal of Chemical Physics* **131**, 014101 (2009).
- ¹⁴ D. Ravnsbæk, Y. Filinchuk, Y. Cerenius, H. Jakobsen, F. Besenbacher, J. Skibsted, and T. Jensen, *Angewandte Chemie International Edition* **48**, 6659 (2009).
- ¹⁵ R. Černý, K. Chul Kim, N. Penin, V. D'Anna, H. Hagemann, and D. S. Sholl, *The Journal of Physical Chemistry C* **114**, 19127 (2010), <http://pubs.acs.org/doi/pdf/10.1021/jp105957r>.
- ¹⁶ D. S. Aidhy and C. Wolverton, *Phys. Rev. B* **83**, 144111 (2011).
- ¹⁷ E. H. Majzoub and V. Ozoliņš, *Phys. Rev. B* **77**, 104115 (2008).
- ¹⁸ D. Ravnsbæk, C. Frommen, D. Reed, Y. Filinchuk, M. Sørby, B. Hauback, H. Jakobsen, D. Book, F. Besenbacher, J. Skibsted, and T. Jensen, *Journal of Alloys and Compounds* **509**, Supplement 2, S698 (2011), Proceedings of the 12th International Symposium on Metal-Hydrogen Systems, Fundamentals and Applications (MH2010).
- ¹⁹ P. Hohenberg and W. Kohn, *Phys. Rev.* **136**, B864 (1964).
- ²⁰ W. Kohn and L. J. Sham, *Phys. Rev.* **140**, A1133 (1965).
- ²¹ G. Kresse and J. Furthmüller, *Phys. Rev. B* **54**, 11169 (1996).
- ²² J. P. Perdew, J. A. Chevary, S. H. Vosko, K. A. Jackson, M. R. Pederson, D. J. Singh, and C. Fiolhais, *Phys. Rev. B* **46**, 6671 (1992).
- ²³ P. E. Blöchl, *Phys. Rev. B* **50**, 17953 (1994).
- ²⁴ G. Kresse and D. Joubert, *Phys. Rev. B* **59**, 1758 (1999).
- ²⁵ H. J. Monkhorst and J. D. Pack, *Phys. Rev. B* **13**, 5188 (1976).
- ²⁶ C. Wolverton, V. Ozoliņš, and M. Asta, *Phys. Rev. B* **69**, 144109 (2004).
- ²⁷ C. Wolverton and V. Ozoliņš, *Phys. Rev. B* **75**, 064101 (2007).
- ²⁸ S. Wei and M. Y. Chou, *Phys. Rev. Lett.* **69**, 2799 (1992).
- ²⁹ D. Wallace, *Thermodynamics of Crystals*, Dover Books on Physics (Dover Publications, 1998).
- ³⁰ J. M. Rickman and R. LeSar, *Annual Review of Materials Research* **32** (2002), 10.1146/annurev.mr.32.010101.100002.
- ³¹ A. R. Akbarzadeh, V. Ozoliņš, and C. Wolverton, *Advanced Materials* **19**, 3233 (2007).
- ³² K. J. Michel, A. R. Akbarzadeh, and V. Ozoliņš, *The Journal of Physical Chemistry C* **113**, 14551 (2009), <http://pubs.acs.org/doi/pdf/10.1021/jp903797v>.
- ³³ Y. Zhang, E. Majzoub, V. Ozoliņš, and C. Wolverton, *Phys. Rev. B* **82**, 174107 (2010).
- ³⁴ K. C. Kim, A. D. Kulkarni, J. K. Johnson, and D. S. Sholl, *Phys. Chem. Chem. Phys.* **13**, 7218 (2011).
- ³⁵ V. Ozolins, A. R. Akbarzadeh, H. Gunaydin, K. Michel, C. Wolverton, and E. H. Majzoub, *Journal of Physics: Conference Series* **180**, 012076 (2009).
- ³⁶ S. Kirklin, B. Meredig, and C. Wolverton, *Advanced Energy Materials*, in press (2012).
- ³⁷ T. H. Mason, X. Liu, J. Hong, J. Graetz, and E. H. Majzoub, *The Journal of Physical Chemistry C* **115**, 16681 (2011), <http://pubs.acs.org/doi/pdf/10.1021/jp203056n>.
- ³⁸ W. Haynes and D. Lide, *CRC Handbook of Chemistry and Physics: A Ready-Reference Book of Chemical and Physical Data*, CRC Handbook of Chemistry and Physics (Taylor & Francis Group, 2010).
- ³⁹ W. Pearson, P. Villars, and L. Calvert, *Pearson's handbook of crystallographic data for intermetallic phases*, Pearson's Handbook of Crystallographic Data for Intermetallic Phases No. v. 2 (American Society for Metals, 1985).
- ⁴⁰ B. F. Decker and J. S. Kasper, *Acta Crystallographica* **12**, 503 (1959).

- ⁴¹ J. Nuss, U. Wedig, A. Kirfel, and M. Jansen, *Zeitschrift für anorganische und allgemeine Chemie* **636**, 309 (2010).
- ⁴² J. P. Vidal and G. Vidal-Valat, *Acta Crystallographica Section B* **42**, 131 (1986).
- ⁴³ J. K. Kang, S. Y. Kim, Y. S. Han, R. P. Muller, and W. A. Goddard, *Appl. Phys. Lett.* **87**, 111904 (2005).
- ⁴⁴ I. Dudenkov and K. Solntsev, *Russian Journal of Inorganic Chemistry* **54**, 1105 (2009), 10.1134/S0036023609070195.
- ⁴⁵ I. Dudenkov and K. Solntsev, *Russian Journal of Inorganic Chemistry* **54**, 1329 (2009).
- ⁴⁶ M. R. Hartman, J. J. Rush, T. J. Udovic, R. C. Bowman Jr., and S.-J. Hwang, *Journal of Solid State Chemistry* **180**, 1298 (2007).
- ⁴⁷ J.-H. Her, M. Yousufuddin, W. Zhou, S. S. Jal-
isatgi, J. G. Kulleck, J. A. Zan, S.-J. Hwang,
R. C. Bowman, and T. J. Udovic, *Inorganic
Chemistry* **47**, 9757 (2008), pMID: 18834192,
<http://pubs.acs.org/doi/pdf/10.1021/ic801345h>.
- ⁴⁸ K. Kuriyama, S. Saito, and K. Iwamura, *Journal of
Physics and Chemistry of Solids* **40**, 457 (1979).
- ⁴⁹ *FIZ Karlsruhe Leibniz Institute for In-
formation Infrastructure*, [http://icsd.fiz-
karlsruhe.de.turing.library.northwestern.edu/icsd/](http://icsd.fiz-
karlsruhe.de.turing.library.northwestern.edu/icsd/).
- ⁵⁰ Y. Zhang, Y. Wang, K. Michel, and C. Wolverton, *Phys.
Rev. B* **86**, 094111 (2012).
- ⁵¹ P. Choudhury, V. R. Bhethanabotla, and E. Stefanakos,
Phys. Rev. B **77**, 134302 (2008).
- ⁵² J. Voss, J. S. Hummelshoj, Z. Lodziana, and T. Vegge,
Journal of Physics: Condensed Matter **21**, 012203 (2009).
- ⁵³ V. Ozolins, E. H. Majzoub, and C. Wolverton, *Phys. Rev.
Lett.* **100**, 135501 (2008).
- ⁵⁴ M. J. van Setten, G. A. de Wijs, and G. Brocks, *Phys.
Rev. B* **77**, 165115 (2008).
- ⁵⁵ T. J. Frankcombe, *The Journal of Phys-
ical Chemistry C* **114**, 9503 (2010),
<http://pubs.acs.org/doi/pdf/10.1021/jp1014109>.
- ⁵⁶ The absolute deviation (δ) between theory and experiment
is defined as $\delta = \frac{|L_{exp} - L_{theory}|}{L_{exp}} \times 100\%$, where L can ei-
ther be the lattice constants or directional coordinates. For
the average absolute deviation, $\delta_{lattice} = (\delta_a + \delta_b + \delta_c)/3$;
 $\delta_{coord} = \sum \delta_i / 3N$, where the summation is over the direc-
tional coordinates of all the atoms, and N is the number
of atoms.
- ⁵⁷ T. J. Frankcombe and G.-J. Kroes, *Phys. Rev. B* **73**,
174302 (2006).
- ⁵⁸ K. Miwa, N. Ohba, S.-i. Towata, Y. Nakamori, and S.-i.
Orimo, *Phys. Rev. B* **69**, 245120 (2004).
- ⁵⁹ Z. Lodziana and T. Vegge, *Phys. Rev. Lett.* **93**, 145501
(2004).
- ⁶⁰ J. Yang, A. Sudik, and C. Wolverton, *The Jour-
nal of Physical Chemistry C* **111**, 19134 (2007),
<http://pubs.acs.org/doi/pdf/10.1021/jp076434z>.
- ⁶¹ J. F. Herbst and L. G. Hector, *Phys. Rev. B* **72**, 125120
(2005).
- ⁶² B. Magyari-Köpe, V. Ozoliņš, and C. Wolverton, *Phys.
Rev. B* **73**, 220101 (2006).
- ⁶³ W. Chase, *JANAF thermochemical tables*, JANAF Ther-
mochemical Tables No. v. 2 (American Chemical Society,
1986).
- ⁶⁴ Assuming that the reaction entropy ΔS is dominated by
the entropy of H_2 gas, i.e. $\Delta S = 130.9 \text{ J}/(\text{K mol } H_2)$, then
according the Van't Hoff equation 6, the target tempera-
ture window of $T = -40 \sim 80^\circ C$ generate a range of $20 \sim 50$
 $\text{kJ}/(\text{mol } H_2)$ reaction enthalpy ΔH at $p = 1 \text{ atm}$.
- ⁶⁵ A. Borgschulte, E. Callini, B. Probst, A. Jain,
S. Kato, O. Friedrichs, A. Remhof, M. Biemann,
A. J. Ramirez-Cuesta, and A. Züttel, *The Jour-
nal of Physical Chemistry C* **115**, 17220 (2011),
<http://pubs.acs.org/doi/pdf/10.1021/jp205566q>.